Adipocyte/macrophage fatty acid binding proteins control integrated metabolic responses in obesity and diabetes

Kazuhisa Maeda,[1,4,5] Haiming Cao,[1,4] Keita Kono,[1] Cem Z. Gorgun,[1] Masato Furuhashi,[1] Kadir T. Uysal,[1] Qiong Cao,[1] Genichi Atsumi,[1,6] Harry Malone,[3] Bala Krishnan,[3] Yasuhiko Minokoshi,[2] Barbara B. Kahn,[2] Rex A. Parker,[3] and Gökhan S. Hotamisligil[1,*]

[1]Department of Genetics and Complex Diseases, Harvard School of Public Health, Boston, Massachusetts, 02115
[2]Division of Endocrinology, Diabetes, and Metabolism, Beth Israel Deaconess Medical Center and Department of Medicine, Harvard Medical School, Boston, Massachusetts, 02215
[3]Bristol-Myers Squibb Pharmaceutical Research Institute, Princeton, New Jersey, 08543
[4]These authors contributed equally to this work.
[5]Present address: Medical Center for Translational Research, Osaka University Hospital, Osaka, Japan.
[6]Present address: Clinical Molecular Biology, Teikyo University, Kanagawa, Japan.
*Correspondence: ghotamis@hsph.harvard.edu

Summary

Fatty acid binding proteins (FABPs) are cytosolic fatty acid chaperones whose biological role and mechanisms of action are not well understood. Here, we developed mice with targeted mutations in two related adipocyte FABPs, aP2 and mal1, to resolve their role in systemic lipid, glucose, and energy metabolism. Mice lacking aP2 and mal1 exhibited a striking phenotype with strong protection from diet-induced obesity, insulin resistance, type 2 diabetes, and fatty liver disease. These mice have altered cellular and systemic lipid transport and composition, leading to enhanced insulin receptor signaling, enhanced muscle AMP-activated kinase (AMP-K) activity, and dramatically reduced liver stearoyl-CoA desaturase-1 (SCD-1) activity underlying their phenotype. Taken together with the previously reported strong protection against atherosclerosis, these results demonstrate that adipocyte/macrophage FABPs have a robust impact on multiple components of metabolic syndrome, integrating metabolic and inflammatory responses in mice and constituting a powerful target for the treatment of these diseases.

Introduction

Adipose tissue plays a critical role in energy homeostasis and an array of endocrine functions. Obesity, characterized by excess accumulation of adipose tissue, is detrimental to many systems and involved in the pathogenesis of multiple human diseases (Saltiel, 2001; Spiegelman and Flier, 2001). These associated pathologies include insulin resistance, type 2 diabetes, dyslipidemia, cardiovascular disease, and fatty infiltration of the liver (Shulman, 2000; Tilg and Diehl, 2000). Currently, more than 64.5% of the adult population in the United States are overweight (Skyler and Oddo, 2002), and obesity and type 2 diabetes are the leading metabolic diseases worldwide (Flegal et al., 1998; Zimmet et al., 2001). The incidence and the impact of this disease cluster, also referred to as metabolic syndrome, have risen to alarming proportions, and there is great need for therapeutic and preventive measures against these major health threats.

The systemic regulation of adiposity is controlled at many levels by mechanisms endogenous both to adipocytes and to paracrine and endocrine links with the central nervous system and other metabolically critical sites such as muscle and liver tissues. Lipids and their derivatives, as well as numerous cytokines and hormones, are important to the function of these networks in health and disease (Friedman and Halaas, 1998; Matsuzawa et al., 1999; Sethi and Hotamisligil, 1999; Shulman, 2000). Obesity is associated with abnormalities of these functional networks at many levels, including aberrant production and/or abnormal function of most of these mediators, leading to an array of associated pathologies (Friedman and Halaas, 1998; Sethi and Hotamisligil, 1999; Shulman, 2000). It is still not fully clear why these pathologies and complications cluster around obesity to establish the phenotype known as metabolic syndrome.

Adipocytes are active sites of lipid metabolism involving storage, mobilization, and transport of lipids as well as utilization of lipid-mediated signaling pathways. These cells contain high levels of a cytosolic fatty acid binding protein (FABP) called aP2 (Bernlohr et al., 1999). It is generally accepted that cytosolic FABPs in general, and aP2 in particular, facilitate the utilization of lipids in metabolic pathways in adipocytes and other cells. It is therefore likely that FABPs serve as a critical link between lipid metabolism, hormone action, and cellular functions in adipocytes and other cell types and thus contribute to systemic energy homeostasis. However, the definitive biology and mechanisms of action of FABPs remain poorly understood. Earlier studies have indicated a role for aP2 in glucose metabolism (Hotamisligil et al., 1996; Scheja et al., 1999; Uysal et al., 2000). Mice deficient in aP2, despite gaining more weight, exhibit a modest increase in insulin sensitivity in the

context of obesity with no protection from fatty liver disease. More recently, a significant impact of this protein on the development of atherosclerosis through modification of macrophage inflammatory responses and cholesterol metabolism was observed (Boord et al., 2002; Makowski et al., 2001). A second FABP isoform, mal1, is also expressed in adipocytes. Mice deficient in mal1 also exhibit a small increase in insulin sensitivity, without changes in total body adiposity (Maeda et al., 2003). Although mal1 is also expressed in macrophages in a similar pattern with aP2, its role, if any, on atherosclerosis has not yet been determined. Although normally found at low levels in adipose tissue, mal1 is strongly upregulated in animals lacking aP2, thus preventing full understanding of FABP function and mechanism of action at this site and systemically (Hotamisligil et al., 1996; Makowski et al., 2001; Scheja et al., 1999). To overcome this limitation and examine the impact of FABPs on adipocyte function and systemic metabolic homeostasis, we developed mice lacking both aP2 and mal1 genes and examined the mechanisms underlying FABP function.

Results

Mice with combined aP2-mal1 deficiency

To address the impact of combined aP2-mal1 deficiency on metabolic control, we have generated an intercross between C57BL/6J-aP2$^{-/-}$ and C57BL/6J-mal1$^{-/-}$ mice (Maeda et al., 2003). Although the estimated genetic distance between these two genes was very close (0.1–0.15 cM), we were able to generate two recombination events between these loci out of 600 offspring in the F2 generation from a cross between aP2-mal1$^{-/+}$ (heterozygous mutant at both loci). The wild-type (wt) and mutant alleles segregated in the expected Mendelian ratios. In double mutant animals, aP2 and mal1 expression were not detectable in various adipose depots (Figure 1A). No compensatory regulation in other major FABPs including liver, brain, intestine, or heart isoforms were observed in adipose tissue of aP2-mal1 null mice (data not shown). There was also no aP2 and mal1 expression in macrophages of double mutant mice (data not shown). In immunoblotting experiments, no aP2 or mal1 protein was detectable in the adipose tissue of aP2-mal1$^{-/-}$ mice (Figure 1B). We also examined the total cytosolic fatty acid binding capacity in adipose tissue of aP2-mal1$^{-/-}$ and wt mice. As shown in Figure 1C, there was a significant reduction in fatty acid binding capacity in aP2-mal1$^{-/-}$ adipose tissue. This reduction was not evident in the single aP2- or mal1-deficient mice, where there was only a small decrease in adipose tissue fatty acid binding capacity in aP2$^{-/-}$ animals and no difference was evident in mal1$^{-/-}$ mice compared to wild-type controls. There was no reduction in fatty acid binding capacity in muscle of aP2-mal1-deficient mice, and the liver fatty acid binding activity was slightly increased as compared to wt (data not shown), suggesting that the loss of fatty acid binding is specific to adipose tissue.

There was no gross apparent abnormality in reproduction, growth, and development of aP2-mal1$^{-/-}$ mice under standard laboratory conditions in either sex. Besides these initial observations, the rest of the detailed experimentation was performed in males. Despite normal axial growth, aP2-mal1$^{-/-}$ mice exhibited a reduction (5.2%) in total body weight compared to controls, suggesting that the absence of these FABPs might influence adiposity (see below). This weight difference was not observed in the aP2$^{-/-}$ or mal1$^{-/-}$ mice on regular diet (Figure 1D). To address the possibility of protection from excess adiposity thoroughly, we placed aP2-mal1$^{-/-}$ mice and wt littermates on a hig-fat (50% of total calories derived from fat) and high-calorie diet (5286 kcal/kg, Bioserve, NJ) along with a control group in each genotype on regular rodent diet. On a high-fat diet, wt control mice developed marked obesity compared to mice fed a regular rodent diet (Figure 1D). However, in the aP2-mal1$^{-/-}$ group, weight gain on the high-fat diet was significantly reduced (15%–16% between ages 8 and 20 weeks, Figure 1D). Again, this pattern differed from the single aP2$^{-/-}$ and mal1$^{-/-}$ mice. Mice with mal1 mutation exhibited a smaller decrease in total body weight, whereas, in aP2$^{-/-}$ animal's body, weight was higher than the wt controls on high-fat diet (Figure 1D).

Adiposity in aP2-mal1-deficient mice

We next assessed whether this reduction in total body weight gain aP2-mal1$^{-/-}$ is related to local and systemic alterations in adiposity by performing whole-body nuclear magnetic resonance (NMR) spectroscopy (Figure 1E) and dual energy X-ray absorption (DEXA) analyses (Figure 1F). In imaging studies by NMR, all fat compartments were clearly reduced in the sections prepared at the levels of neck, around kidneys, abdominal region, and subcutaneous depots of the aP2-mal1$^{-/-}$ mice compared to the wt controls on both regular and high-fat-diet-fed animals (Figure 1E). In fact, the body composition of wt mice on regular diet and aP2-mal1$^{-/-}$ mice on high-fat diet appeared quite similar. To investigate the level of total systemic reduction in adiposity, we next examined total body composition by DEXA and proton NMR (Sjogren et al., 2001). There was no significant difference in total body composition in aP2$^{-/-}$ or mal1$^{-/-}$ mice compared to wt controls on either regular or high-fat diet (Figure 1F). However, DEXA analyses demonstrated significantly reduced total body adipose mass in aP2-mal1$^{-/-}$ mice both on regular and high-fat diet (Figure 1F). These results were also confirmed with total body proton NMR analysis (Razani et al., 2002), which exhibited 22% and 25.8% reduction in total body fat in aP2-mal1$^{-/-}$ mice compared to wt controls on regular and high-fat diet, respectively.

Energy metabolism in aP2-mal1$^{-/-}$ mice

The two major components contributing to the systemic energy balance and adiposity are energy intake and expenditure. To identify potential contributors to body weight reduction, food intake and energy expenditure were examined in aP2-mal1$^{-/-}$ and wt groups. Despite being leaner, the aP2-mal1$^{-/-}$ mice had no reduction in total daily food intake. In fact, these animals consumed slightly more food, although this difference was statistically insignificant between genotypes on either regular or high-fat diet (see Figure S1A in the Supplemental Data available with this article online, and data not shown). When corrected for body weight, the increase in total food intake became more evident (Figure S1A). During the period of food intake measurements, body weight difference was again apparent between genotypes (Figure S1B). There was also no difference in rectal temperature (Figure S1C) or fecal lipid content (Figure S1D) between genotypes, ruling out fever or intestinal malabsorption as underlying causes of reduced adi-

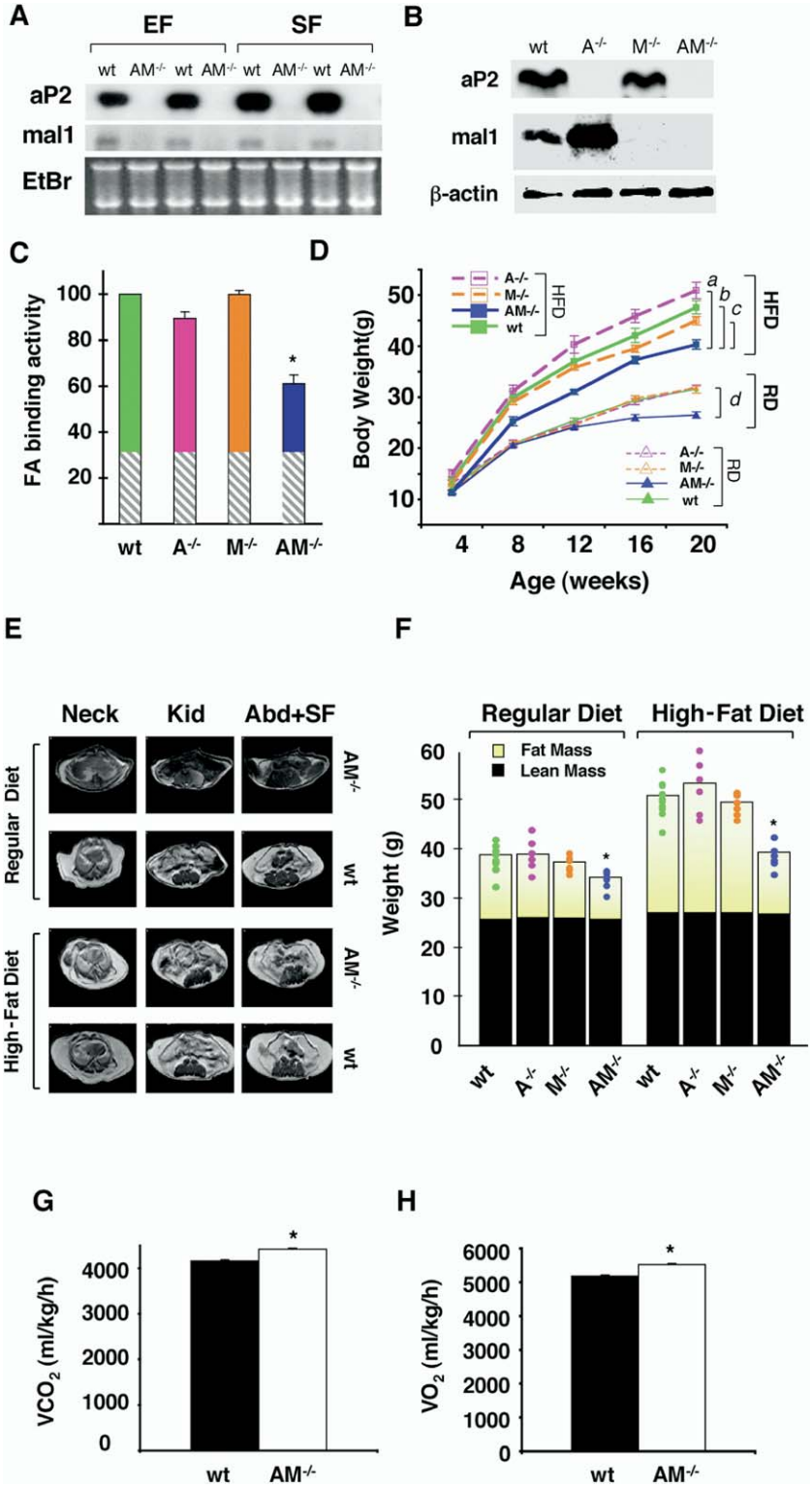

Figure 1. Total adiposity, adipose depot distribution, and expression of FABPs in aP2-mal1-deficient mice

A) Lack of aP2 and mal1 mRNA expression in aP2-mal1-deficient mice. Probes for aP2 and mal1 FABP isoforms were hybridized with total RNA from epididymal (EF) and subcutaneous fat (SF) of 16-week-old, wild-type (wt), and aP2-mal1-deficient ($AM^{-/-}$) mice. Loading and integrity of RNA is shown with EtBr staining. **B)** Lack of adipose tissue aP2 and mal1 proteins in aP2-mal1-deficient mice. Immunoblots with isotype-specific antibodies showing the absence of aP2 and/or mal1 proteins in wt, $aP2^{-/-}$ ($A^{-/-}$), $mal1^{-/-}$ ($M^{-/-}$), and aP2-mal1-deficient mice. **C)** Adipose fatty acid binding activity of wt (green), $A^{-/-}$ (pink), $M^{-/-}$ (orange), and $AM^{-/-}$ (blue) mice. Values for each mutant strain are expressed as percentage of wt. Textured part of each column represents predicted nonspecific binding (see Supplemental Experimental Procedures). **D)** Growth curves of wt (green), $A^{-/-}$ (pink), $M^{-/-}$ (orange), and $AM^{-/-}$ (blue) mice on regular (RD) or high-fat diet (HFD). Obesity is induced by high-fat diet starting from 3 weeks of age. a = $AM^{-/-}$ is statistically significantly different from $A^{-/-}$; b = $AM^{-/-}$ is statistically significantly different from wt; c = $AM^{-/-}$ is statistically significantly different from $M^{-/-}$; d = $AM^{-/-}$ is statistically significantly different from wt, $A^{-/-}$, and $M^{-/-}$ mice. **E)** Nuclear magnetic resonance (NMR) sections obtained from the same groups of mice shown in (**D**) at 16 weeks of age. **F)** Total body composition analysis by dual energy X-ray absorptiometry (DEXA). Black bars indicate lean body mass, and the yellow bars indicate fat mass. Data on all mice used in DEXA experiments are also shown on the upper portion of the graph by filled circles. **G)** CO_2 production and (**H**) O_2 consumption of $AM^{-/-}$ and wt mice determined by indirect calorimetry. Error bars represent the SEM. Asterisk, $p < 0.05$.

posity in FABP-deficient animals.

We next determined whether differences in energy expenditure in aP2-mal1-deficient animals could account for the differences in adiposity by performing indirect calorimetry studies and determination of physical activity. In these studies, aP2-mal1-deficient mice exhibited similar rates of physical activity in continuous 48 hr period measurements (Figure S1E). However, there was a significant increase in the rates of carbon dioxide production (Figure 1G) and oxygen consumption (Figure 1H) in aP2-$mal1^{-/-}$ mice compared to wt controls. Taken

together, these data demonstrate that the primary metabolic mechanism underlying the reduction in adiposity in aP2-mal1$^{-/-}$ mice is increased energy expenditure.

Adipose tissue, lipid transport and distribution, and adipocytokines in aP2-mal1-deficient mice

There was no significant difference in the extent of adipocyte differentiation in aP2-mal1$^{-/-}$ mouse embryonic fibroblasts compared to wt or heterozygous cells (data not shown). In light of these observations, we next considered the possibility that the combined lack of aP2 and mal1 alters the lipid profiles in tissues due to their differential affinity and transport properties. To address this question, we isolated the fatty acid fraction from two different adipose tissue depots and quantified individual fatty acids. We also performed parallel fatty acid profiling experiments in muscle and liver tissues and serum. These experiments revealed significant differences in fatty acid distribution between wt and aP2-mal1$^{-/-}$ mice (Figures 2A and 2B). Among saturated fatty acids, accumulation of shorter chain fatty acids such as myristic acid (14:0) was favored in aP2-mal1$^{-/-}$ adipose and muscle tissues compared to stearic (18:0) or palmitic acid (16:0). Strikingly, liver exhibited the complete opposite pattern of fatty acid distribution between aP2-mal1$^{-/-}$ mice and wt controls. Among monounsaturated fatty acids, the ratios strongly favored myristoleic (14:1n-5c) and palmitoleic (16:1n-7c) acid in adipose and muscle tissues (Figure 2B). The lipid profiles were similar between the two adipose tissue depots studied. This distribution was not present in liver or serum, where monounsaturated fatty acid ratio was extremely low compared to longer chain length fatty acids in aP2-mal1$^{-/-}$ mice. In a separate experiment, we also measured the adipose tissue lipid composition of all of the same fractions quantitatively and obtained similar results in lipid distribution (data not shown).

Next, we examined whether the adipocyte FABPs regulate fatty acid transport properties, which might underlie the alterations observed in lipid composition in aP2-mal1$^{-/-}$ adipose tissue. Typically, fatty acid uptake experiments are performed by palmitic acid (16:0). When we also used this fatty acid in initial experiments, we have not observed any differences between genotypes (Figure 2C). As adipose tissue palmitic acid levels are also similar between genotypes, we next asked whether fatty acid uptake differs between aP2-mal1-deficient and wt adipocytes for fatty acids with different chain lengths. Interestingly, these experiments demonstrated that the uptake of stearic acid (18:0) was significantly reduced in aP2-mal1-deficient adipocytes. In contrast, fatty acid uptake was increased for lauric acid (12:0). These data provide a potential mechanism for the alterations in lipid composition in adipose tissue via chain length-selective regulation of fatty acid trafficking in adipocytes. In biochemical measurements of steady-state serum lipids, we observed a modest decrease in circulating triglycerides and a modest increase in free fatty acid concentrations (Table S1). These changes were observed in animals on both regular and high-fat diets. There was no significant alteration in serum glycerol or total cholesterol levels between genotypes.

We also investigated the expression patterns of several adipose-derived hormones in adipose tissues from mice on high-fat diet to determine the impact of these compositional changes on adipocytokines. There were reductions in the expression of adiponectin (62%), leptin (52%), and TNFα (70%) mRNAs in aP2-mal1$^{-/-}$ mice (Figure 2D) in the epididymal adipose depot compared to wt controls. Serum leptin level was also significantly (63.0%) reduced in aP2-mal1$^{-/-}$ mice (13.04 ± 1.1 versus 4.8 ± 0.5 ng/ml in wt and aP2-mal1$^{-/-}$ mice, respectively, $p < 0.005$, Figure 2E). Interestingly, the serum level of adiponectin was also decreased (15.1%) in the aP2-mal1$^{-/-}$ animals (25.18 ± 1.0 versus 21.4 ± 1.1 μg/ml in wt and aP2-mal1$^{-/-}$ mice, respectively, $p < 0.05$, Figure 2F). This is surprising, since adiponectin levels typically correlate negatively with body weight (Arita et al., 1999). Finally, there was no detectable circulating TNFα in the aP2-mal1$^{-/-}$ mice, whereas, in wt mice on high-fat diet, TNFα protein was detectable in serum (27.3 ± 7 pg/ml). These results demonstrate that FABP deficiency results in alterations in lipids and adipocytokines, the two major classes of metabolic regulators derived from adipose tissue. These changes also create a milieu that might have a strong impact on systemic insulin action, which is addressed below.

Protection against insulin resistance in aP2-mal1$^{-/-}$ mice

Rising blood glucose and insulin levels in animals on high-fat diet are an indicator of obesity-induced insulin resistance and development of type 2 diabetes. Measurement of blood glucose levels demonstrated that obese wt mice developed hyperglycemia compared to lean controls (330 ± 7.2 versus 197 ± 6.1 mg/dl, $p < 0.001$). However, on the high-fat diet, aP2-mal1$^{-/-}$ mice had significantly lower blood glucose concentrations compared to wt controls (Figure 3A). In fact, throughout the experiment, the blood glucose levels in aP2-mal1$^{-/-}$ mice on high-fat diet were indistinguishable from those of lean wt animals on regular diet (196 ± 5.7 verus 197 ± 6.1 mg/dl). Blood glucose levels on regular diet were also lower (163 ± 5.4 mg/dl), although to a lesser extent, in the aP2-mal1$^{-/-}$ mice compared to wt controls. Wt mice on high-fat diet developed hyperinsulinemia compared to those on regular diet (3.2 ± 0.7 versus 0.65 ± 0.2 ng/ml $p < 0.001$). Blood insulin levels in aP2-mal1$^{-/-}$ mice were significantly lower throughout the experimental period compared to wt controls (Figure 3B) and were indistinguishable from those of wt lean mice (0.66 ± 0.1 versus 0.65 ± 0.2). Hence, these results indicate that the aP2-mal1-deficient animals might be protected from the development of high-fat-diet-induced insulin resistance and diabetes.

To further investigate systemic insulin sensitivity, we performed insulin (ITT) and glucose (GTT) tolerance tests in aP2-mal1$^{-/-}$ mice and wt controls. Insulin resistance was evident in wt mice upon high-fat diet. As shown in Figure 3C, the hypoglycemic response to insulin in aP2-mal1$^{-/-}$ mice on high-fat diet was indistinguishable from control animals on regular diet. GTT also revealed a higher degree of hyperglycemia in wt animals throughout the experiment, compared to aP2-mal$^{-/-}$ mice on high-fat diet (Figure 3D). In this test, the responses recorded in aP2-mal1$^{-/-}$ mice did not reach those of lean controls. While these responses were also improved in aP2$^{-/-}$ and mal1$^{-/-}$ mice on high-fat diet, these changes were significantly smaller in magnitude (Figures 3E and 3F). The increase in insulin sensitivity in ITT was most dramatic in aP2-mal1$^{-/-}$ mice on high-fat diet. The magnitude of increase in insulin responsiveness in the aP2$^{-/-}$ mice (38%) was smaller than that in aP2-mal1$^{-/-}$ mice (55%) but greater than the mal1$^{-/-}$ animals (15%) on the high-fat diet (Figure 3E). Similar to the results of ITT, the magnitude of increase in glucose disposal relative to the wt controls

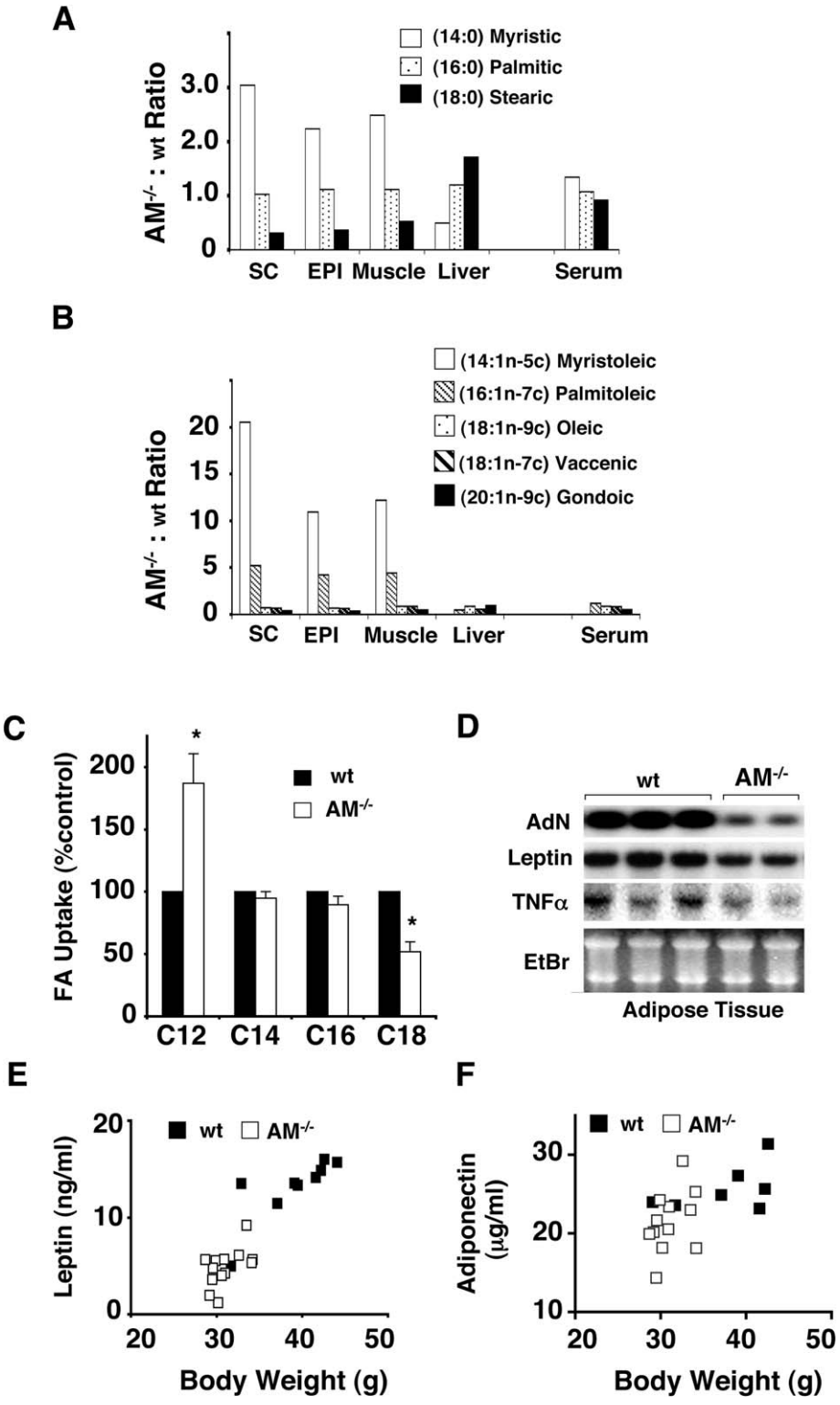

Figure 2. Adipocyte fatty acid uptake, gene expression, and tissue lipid composition in aP2-mal1-deficient mice

Saturated (**A**) and nonsaturated (**B**) fatty acid composition in subcutaneous (SC) and epididymal (EPI) adipose, muscle, liver tissues, and serum in aP2-mal1-deficient ($AM^{-/-}$) mice compared to wild-type (wt) controls. **C)** Uptake of lauric (C12), myristic (C14), palmitic (C16), and stearic (C18) by primary adipocytes isolated from wt or $AM^{-/-}$ mice. Values for FABP-deficient mice expressed as percentage of wt. Error bars represent the SEM. Asterisk, $p < 0.01$. **D)** Steady-state mRNA expression patterns in epididymal adipose tissues of $AM^{-/-}$ and wt mice. Gene expression is determined by Northern blot analyses as in Figure 1. **E)** Serum level of leptin and (**F**) adiponectin plotted against body weight at 12 weeks of age on high-fat diet in wt and $AM^{-/-}$ mice.

in the $aP2^{-/-}$ mice (28%) was smaller than the aP2-$mal1^{-/-}$ mice (45%) but greater than the $mal1^{-/-}$ animals (9%) on high-fat diet (Figure 3D). These results demonstrate that the combined deficiency of aP2 and mal1 resulted in a significant protection from high-fat-diet-induced insulin resistance and type 2 diabetes.

Muscle lipids, AMP-activated kinase activity, and insulin sensitivity in ap2-mal1-deficient mice

The reduction in body weight and adiposity in FABP-deficient mice could have an influence on the insulin sensitivity. However, the impact of FABP deficiency on systemic insulin sensitivity is disproportionate to its effects on body weight and

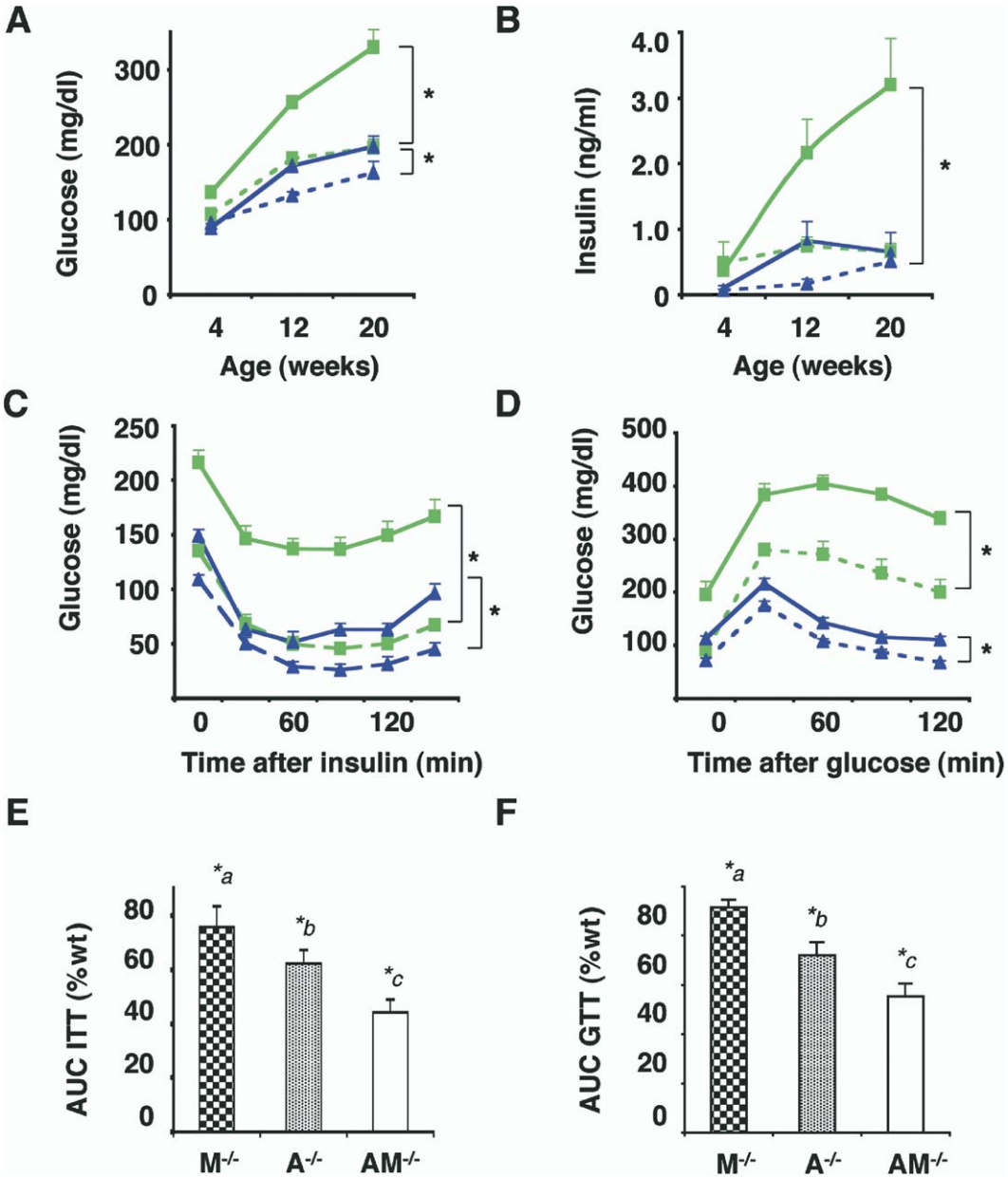

Figure 3. Glucose metabolism in aP2-mal1-deficient mice

Blood glucose (**A**) and insulin (**B**) levels in wt (blue triangle solid line, n = 17) and aP2-mal1-deficient ($AM^{-/-}$, blue triangle dashed line, n = 14) mice on regular diet and wt (green square solid line, n = 12) and $AM^{-/-}$ (green square dashed line, n = 13) mice on high-fat diet. Glucose and insulin were measured after 6 hr daytime food withdrawal. Insulin (**C**) and glucose (**D**) tolerance tests performed on wt and $AM^{-/-}$ mice on regular and high-fat diet. Asterisk, $p < 0.05$. Insulin (**E**) and glucose (**F**) tolerance test in all mutants expressed as integrated area under the glucose disposal curves (AUC) for each genotype relative to wt controls on high-fat diet. Experiments are performed on 14–16 weeks of age at fasting state, n = 6–8 in each group. Error bars represent the SEM. *a = $M^{-/-}$ is statistically significantly different from wt; *b = $A^{-/-}$ is statistically significantly different from wt and $M^{-/-}$; *c = $AM^{-/-}$ is statistically significantly different from wt, $A^{-/-}$, and $M^{-/-}$ mice.

hence should involve an independent direct impact on insulin action. The dramatic increase in insulin sensitivity as well as changes in energy homeostasis, lipid profiles, and adipocytokines all point to the involvement of muscle tissue in the phenotype of FABP-deficient animals. A feasible mechanism in this context is the alterations of lipid content and/or composition of the muscle (as shown earlier), which in turn activate insulin receptor signaling cascades and/or other pathways related to energy expenditure. To address this model, we first examined muscle lipid content. In fact, total muscle triglyceride content was significantly lower (Figure 4A) in the aP2-$mal1^{-/-}$ mice compared to wt controls (0.044 ± 0.006 versus 0.066 ± 0.01 mg/g, respectively, $p < 0.005$). As stated before, there was also a shift in the distribution of saturated fatty acids favoring in the aP2-$mal1^{-/-}$ animals the shorter chain myristic (14:0) versus longer chain stearic (18:0) acid (Figure 2A). We reasoned that this lipid environment would be favorable to insulin action and hence examined insulin sensitivity in isolated muscle strips and

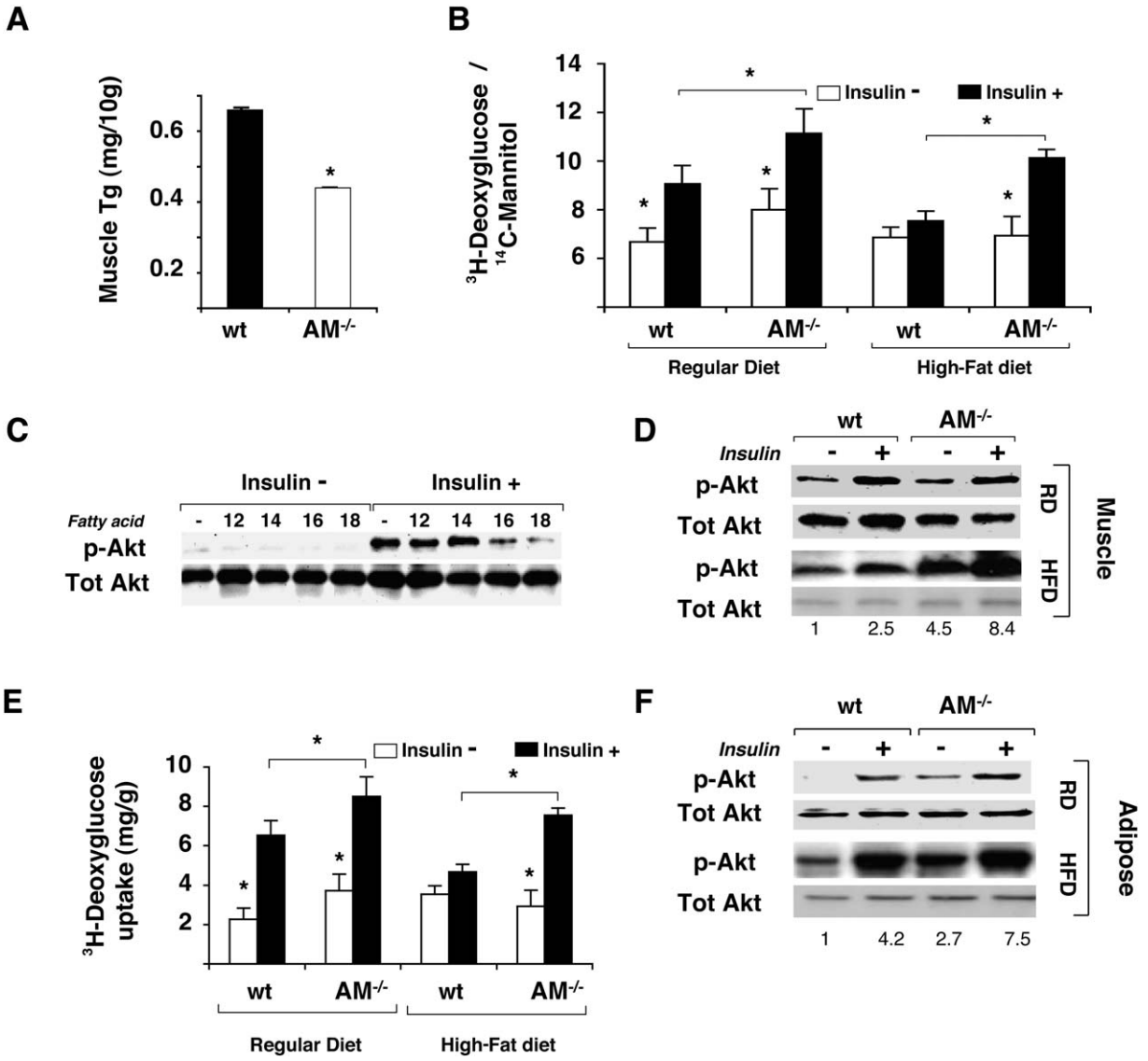

Figure 4. Tissue lipid content and insulin responsiveness in aP2-mal1 deficiency

A) Triglyceride content of skeletal muscle obtained from aP2-mal1$^{-/-}$ (AM$^{-/-}$) and wt mice on high-fat diet.

B) Baseline and insulin-stimulated glucose transport in isolated muscle strips obtained from aP2-mal1$^{-/-}$ (AM$^{-/-}$) and wild-type (wt) mice on both regular and high-fat diet.

C) The effects of fatty acid chain length on baseline and insulin-stimulated phosphorylation of Akt in cultured C2C12 myocytes.

D) Baseline and insulin-stimulated phosphorylation of Akt in the muscle tissue of AM$^{-/-}$ and wt mice on regular (RD) and high-fat diet in vivo (HFD). The numbers under the blot show the quantitation of the phospho-Akt signal on high-fat diet in phosphoimager.

E) Baseline and insulin-stimulated glucose transport in isolated adipocytes from AM$^{-/-}$ and wt mice on both regular and high-fat diet.

F) Baseline and insulin-stimulated Akt phosphorylation in the adipose tissues of AM$^{-/-}$ and wt mice on regular and high-fat diet in vivo. The numbers under the blot show the quantitation of the phospho-Akt signal on high -fat diet in phosphoimager. Error bars represent the SEM. Asterisk, $p < 0.05$.

muscle tissues obtained from wt and aP2-mal1$^{-/-}$ mice. In experiments with isolated primary muscle strips from wt and aP2-mal1$^{-/-}$ mice, we observed a significant increase in insulin-stimulated glucose transport capacity in aP2-mal1$^{-/-}$ muscle cells (Figure 4B). This increase was evident in muscles obtained from mice under both regular and high-fat diet (Figure 4B) but more striking in the latter, indicating essentially complete rescue of glucose transport capacity in aP2-mal1$^{-/-}$ cells despite exposure to high-fat diet. We next asked whether insulin action in muscle cells is altered as a function of the lipid environment observed in aP2-mal1$^{-/-}$ muscle tissue. To investigate this question, we incubated cultured muscle cells with a variety of lipids and examined insulin-stimulated phosphorylation of Akt (Figure 4C). These experiments clearly showed that insulin-stimulated phosphorylation of Akt was higher in the presence of shorter chain (12:0 and 14:0) fatty acids and strongly inhibited in the presence of longer chain (16:0 and 18:0) fatty acids (Figure 4C). These findings demonstrate that lipid composition in the aP2-mal1$^{-/-}$ muscle tissue was highly favorable for insulin action. We also studied insulin-stimulated

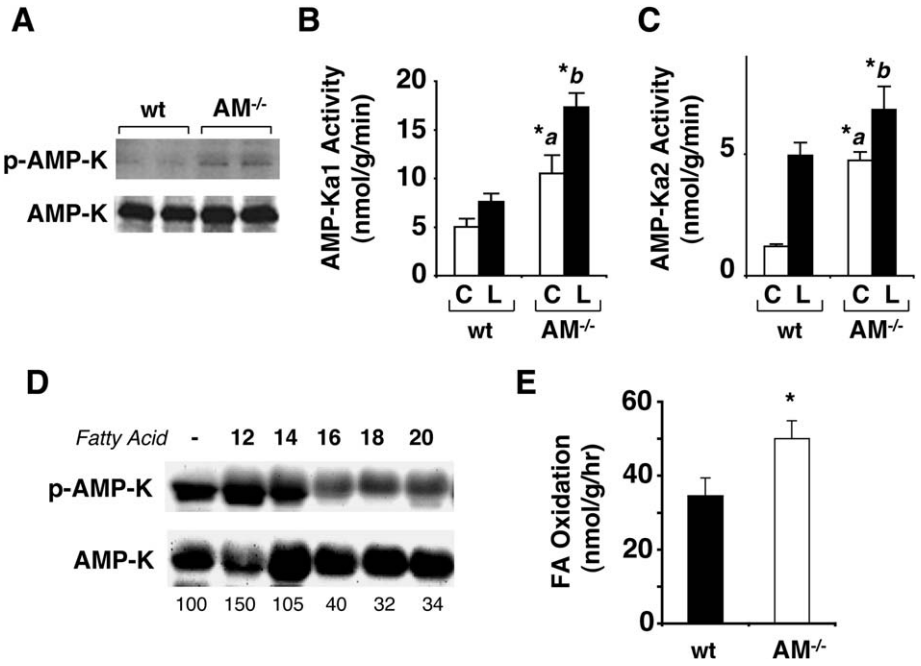

Figure 5. Phoshorylation of AMP-activated kinase and fatty acid oxidation in muscle

A) Phosphorylation and total protein levels of AMP-K in soleus muscle of aP2-mal1$^{-/-}$ (AM$^{-/-}$) and wild-type (wt) mice with high-fat-diet-induced obesity. These experiments reflect baseline activity at 16 wError bars represent theeeks of age.

B) AMP-K-α1 activity in soleus muscle following 15 min saline (C) or leptin (L) treatment in AM$^{-/-}$ and wt mice with high-fat-diet-induced obesity (n = 5–6 for each condition).

C) AMP-K-α2 activity in soleus muscle under the same conditions in (**B**). Asterisk, $p < 0.05$ *a = significantly different from baseline activity in wt controls; *b = significantly different from both baseline and stimulated activity in wt controls and also from baseline activity in AM$^{-/-}$ mice.

D) The effects of fatty acid chain length on phosphorylation of AMP-K in cultured L6 myocytes. AMP-K phosphorylation is detected by a phospho-specific antibody.

E) Fatty acid oxidation in soleus muscle isolated from AM$^{-/-}$ and wt mice. Error bars represent the SEM. Asterisk, $p < 0.05$.

phosphorylation of Akt in the muscle tissue of aP2-mal1$^{-/-}$ and control mice on both regular and high-fat diet (Figure 4D). The phospho-Akt levels were similar between genotypes in mice on regular diet except for a small increase in baseline Akt phosphorylation in aP2-mal1$^{-/-}$ mice. There was, however, a significant increase in phosphorylation of muscle Akt in aP2-mal1-deficient animals on high-fat diet both before and following insulin stimulation (Figure 4D). Similar results were also obtained in adipose tissue, where both insulin-stimulated glucose transport and Akt activation were strikingly increased in aP2-mal1-deficient animals (Figures 4E and 4F). In adipose tissue, the increase in baseline Akt phosphorylation in the lean aP2-mal1$^{-/-}$ animals appeared more evident. These data clearly demonstrate that, at the molecular level, aP2-mal1 deficiency resulted in striking protection from high-fat-induced inhibition of insulin action in muscle and adipose tissues.

An important energy sensor in skeletal muscle is the AMP-activated kinase (AMP-K). Interestingly, this kinase is targeted by leptin, and its activation is a potential protective mechanism against lipid accumulation. The fatty acid oxidation induced in muscle by leptin and adiponectin (Fruebis et al., 2001; Muoio et al., 1997) and potentially the protection against obesity and diabetes might be related, at least in part, to their ability to induce AMP-activated protein kinase activity (Minokoshi et al., 2002; Winder and Hardie, 1999; Yamauchi et al., 2001). We therefore determined whether AMP-K is differentially phosphorylated in muscle tissue of aP2-mal1$^{-/-}$ mice and wt controls. Levels of total and phosphorylated AMP-K were measured in the soleus muscle by immunoblot analyses (Figure 5A). Quantification of immunoblot analyses demonstrated a significant 2-fold increase in the amount of phosphorylated AMP-K in soleus muscle from obese aP2-mal1$^{-/-}$ mice compared to wt controls.

To examine the level of activation of AMP-K in muscle in response to leptin, we administered recombinant leptin (1 mg/kg i.v.) to age- and sex-matched wt and aP2-mal1$^{-/-}$ mice on high-fat diet. We then isolated the soleus muscle and determined the ability of leptin to activate this kinase. Leptin administration increased the AMP-K-α1 activity 50% over baseline in wt mice (Figure 5B). At the baseline, aP2-mal1$^{-/-}$ mice exhibited significantly increased (2.1-fold) AMP-K-α1 activity compared to wt mice. In aP2-mal1$^{-/-}$ animals, leptin further stimulated the AMP-K-α1 activity (70% over baseline) in soleus muscle, which was significantly higher (2-fold) than leptin-stimulated AMP-Kα1 activity in wt controls (Figure 5B). Leptin also stimulated the AMP-Kα2 activity (4.1-fold over baseline) in wt animals (Figure 5C). As reported, this was more potent compared to leptin's ability to stimulate the AMP-Kα1 isoform (Minokoshi et al., 2002). In aP2-mal1$^{-/-}$ animals, baseline AMP-Kα2 activity in soleus muscle was significantly higher than wt animals (3.9-fold) and already reached the levels observed in the leptin-treated wt mice. Leptin treatment further stimulated AMP-Kα2 to even higher levels over the already increased baseline activity in aP2-mal1-deficient mice (Figure 5C). We next asked whether the mechanism underlying the increase in AMP-K activity might be the alterations in lipid composition. To approach this question, we exposed cultured muscle cells to fatty acids with various chain lengths and determined the phosphorylation of AMP-K (Figure 5D). These experiments demonstrated that phosphorylation of AMP-K was significantly higher in the presence of shorter chain (12:0 and 14:0) fatty acids and inhibited in the presence of longer chain (16:0 and 18:0) fatty acids (Figure 5D). Based on these observations, we postulated that these alterations might lead to enhanced fatty acid oxidation in muscle, which would be consistent with increased metabolic rate and reduced body weight. To address this, we determined fatty acid oxidation in soleus muscle strips isolated from aP2-mal1$^{-/-}$ mice and wt control animals. These experiments demonstrated significantly increased capability of

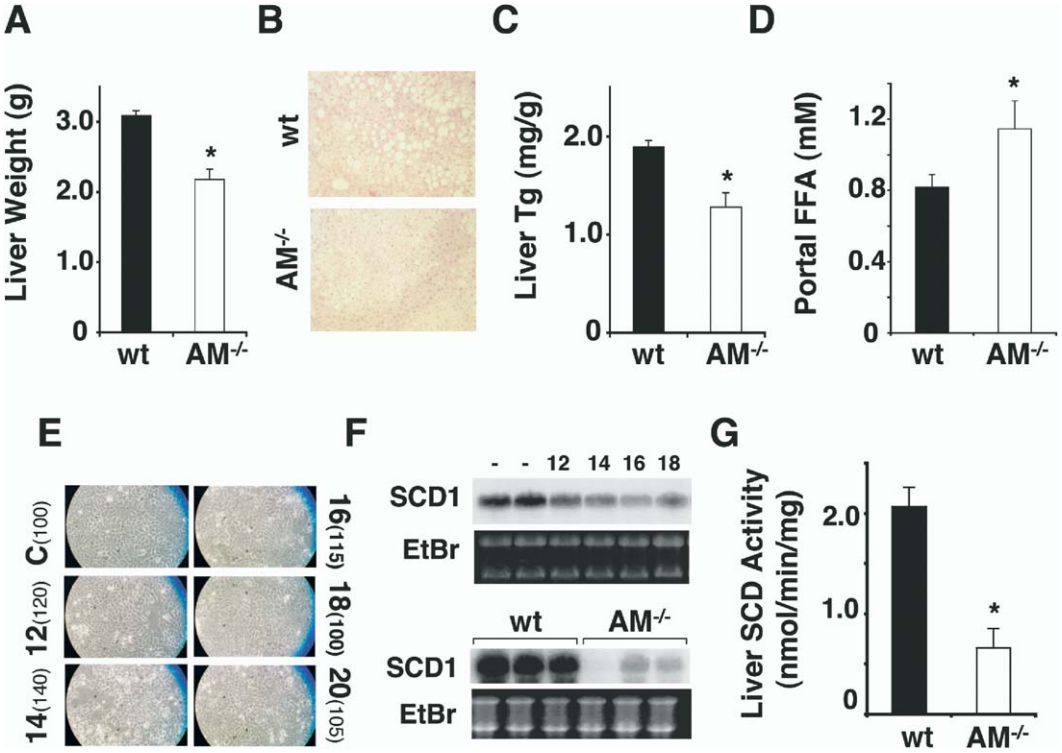

Figure 6. FABPs role in liver lipid metabolism, hepatosteatosis, and SCD-1 activity

A) Total wet weight of liver tissue obtained from aP2-mal1$^{-/-}$ (AM$^{-/-}$) and wt mice on high-fat diet.

B) Representative hematoxylin and eosin (H&E) stains of liver tissue (×100) sections from AM$^{-/-}$ and wt mice on high-fat diet prepared at 20 weeks of age.

C) Triglyceride content of liver tissue obtained from AM$^{-/-}$ and wt mice on high-fat diet.

D) Portal concentration of free fatty acids in AM$^{-/-}$ and wt mice on high-fat diet.

E) The effects of fatty acid chain length on lipid accumulation in Fao liver cells. Direct micrographs are shown after 48 hr treatment with the indicated fatty acids. The quantitation in each experiment is shown as a percent of control in parenthesis.

F) Stearoyl-CoA desaturase-1 (SCD-1) expression in Fao cells treated with lipids and in liver tissue of AM$^{-/-}$ and wt mice on high-fat diet.

G) Total SCD activity in liver tissue of AM$^{-/-}$ and wt mice on high-fat diet. Error bars represent the SEM. Asterisk, $p < 0.05$.

aP2-mal1$^{-/-}$ muscle for fatty acid oxidation (Figure 5E). Taken together, these data indicate that lipids of various lengths differentially impact muscle AMP-K activity, consistent with the observed muscle tissue lipid composition, increased activation of AMP-K, and enhanced fatty acid oxidation in aP2-mal1-deficient animals.

Protection against fatty liver disease in aP2-mal1-deficient mice

The weight of the liver was reduced in the aP2-mal1$^{-/-}$ animals on high-fat diet (Figure 6A). Consistent with the reduction in liver weight, histological examination of liver sections revealed a dramatic reduction in fatty infiltration in aP2-mal1$^{-/-}$ mice compared to the wt animals (Figure 6B). In fact, the histopathology of aP2-mal1$^{-/-}$ livers on high-fat diet was indistinguishable from livers of mice on regular diet.

Accumulation of lipids in the liver may involve several pathways. To approach the mechanisms underlying the protection from fatty liver disease in the aP2-mal1$^{-/-}$ mice, we first biochemically determined the liver triglyceride content. These experiments demonstrated significantly lower liver tissue triglyceride accumulation (Figure 6C) in the aP2-mal1$^{-/-}$ mice compared to wt controls (1.28 ± 0.14 versus 1.89 ± 0.07 mg/g, respectively, $p < 0.05$). This significant reduction in liver triglyceride content and hepatosteatosis was not evident in aP2$^{-/-}$ or mal1$^{-/-}$ mice (data not shown). Interestingly, the portal free fatty acid levels were even higher in the aP2-mal1$^{-/-}$ mice compared to wt controls on high-fat diet (Figure 6D). This, along with the alteration in the liver lipid profile, suggests an intracellular hepatic mechanism accounting for the lack of lipid accumulation in liver cells.

The lipid profile seen in liver with accumulation of longer chain fatty acids such as stearic acid is striking, since this pattern was the opposite of lipid distribution detected in adipose and muscle tissues where there was accumulation in favor of shorter chain fatty acids. To test the potential impact of this lipid distribution on the development of hepatosteatosis, we first tested the ability of lipids with various chain lengths to accumulate in cultured liver cells. These experiments demonstrate that fatty acid chain length is inversely correlated with the ability to accumulate lipids in cultured liver cells where longer chain (16:0 and 18:0) fatty acids essentially lacked the ability to induce hepatosteatosis, therefore supporting the hypothesis that lipid metabolism as well as composition might underlie the lack of fatty liver disease in aP2-mal1-deficient mice (Figure 6E). The lipid distribution pattern observed in the

livers of aP2-mal1$^{-/-}$ mice led us to postulate that likely loci that are affected might be fatty acid synthase (FAS) and/or stearoyl-CoA desaturase-1 (SCD-1). Interestingly, SCD-1 expression in liver cells was strongly suppressed by fatty acids but without the same clear and dramatic effect of chain length seen in muscle (Figure 6F). Examination of SCD-1 expression in the liver tissues of aP2-mal1$^{-/-}$ mice and wt controls on high-fat diet also demonstrated a striking defect in the expression of SCD-1 in the liver tissue of aP2-mal1$^{-/-}$ animals (Figure 6F). This reduction in SCD-1 mRNA expression was associated with a significant decrease in liver SCD activity (Figure 6G). In contrast, there was no reduction in SCD activity in adipose (3.17 ± 0.32 versus 2.89 ± 0.51 in wt and aP2-mal1$^{-/-}$ mice, respectively) or muscle tissues (0.28 ± 0.04 versus 0.25 ± 0.04 in wt and aP2-mal1$^{-/-}$ mice, respectively). Interestingly, SCD-1 is recently reported to be the predominant peripheral target of leptin in liver. Upon treatment with leptin, or in ob/ob mice where leptin expression is transgenically reconstituted, SCD-1 expression in liver is strongly suppressed. However, the level of regulation seen in aP2-mal1$^{-/-}$ mice is greater than what has been achieved through leptin administration or transgenic leptin production (Cohen et al., 2002; Soukas et al., 2000), suggesting that its regulation may not be entirely related to leptin action at this site.

Finally, we examined the expression patterns of other molecules that are critical in liver lipid metabolism, including the SREBP family of transcription factors, acetyl-CoA carboxylase 1 (ACC-1), and fatty acid synthase (FAS), to be able to construct a better mechanistic model (Table S2). Among all of the genes examined, the most dramatic regulation was for SCD-1 (96% reduction in aP2-mal1$^{-/-}$ mice). Interestingly, these experiments also demonstrated reduction (70%) in liver SREBP1c expression in aP2-mal1-deficient mice. Consistent with this, we also detected moderate decreases in the expression of a number of additional SREBP1 target genes critical in fatty acid metabolism, including ACC-1, FAS, ELOVL6, SPOT14, HMG-CoA reductase, and HMG-CoA synthase (Table S2). In contrast, no change was evident in the expression levels of SREBP2, DGAT1, or mGPAT.

Discussion

Fatty acids have long been seen as critical components of the pathogenesis of obesity and its associated disorders. However, the mechanisms by which these or other lipids mediate these abnormalities remain unclear. Our findings in this study demonstrate that FABPs are critical in the interface between cellular lipid trafficking and homeostasis and the peripheral signaling pathways that are central to obesity and its associated pathologies. The deletion of two FABPs, aP2 and mal1, in mice causes significant changes in lipid and hormone profiles and leads to significant protection against obesity, insulin resistance, type 2 diabetes, and fatty liver disease.

In FABP-deficient animals, there is an increase in the ratio of shorter chain (C14) to longer chain (C18) fatty acids in adipose and muscle tissues. This pattern is reflected in circulating lipids but reversed in liver. We have presented several intermediary mechanisms in this lipid environment that underlie the phenotype of the mice. First, we demonstrated the differential impact of exposure to fatty acids of different chain length on muscle insulin receptor signaling. These results are in line with previous reports indicating the inhibitory effects of long chain fatty acids on insulin action (Chavez and Summers, 2003). Consistent with these findings, basal and insulin-stimulated phosphorylation of Akt in FABP-deficient mice is also significantly increased in adipose and muscle tissues, accompanied by increased insulin-stimulated glucose uptake at both sites. Second, we demonstrate that the lipid composition of muscle is altered to favor shorter chain length fatty acids. This composition supports higher levels of AMP-K activity in cultured cells and, consistent with these observations, there is increased basal and stimulated muscle AMP-K activity, fatty acid oxidation, and increased energy expenditure in FABP-deficient mice. Consequently, the overall triglyceride content of the muscle, a well-established indicator of lipotoxicity, is also reduced in aP2-mal1$^{-/-}$ animals, although the magnitude of this reduction is moderate. Whether alterations in lipid uptake in muscle also contribute to the muscle lipid composition and metabolism remains to be determined. Third, we demonstrated a significant reduction in liver SCD-1 expression and activity in FABP-deficient animals accompanied by increased longer chain fatty acids and striking resistance to fatty liver disease upon exposure to a high-fat diet. These changes occur despite higher systemic and portal fatty acid input. We also demonstrated the differential impact of exposure to fatty acids of different chain length on SCD-1 expression and the capacity to induce lipid accumulation in liver cells. The reduction in SCD-1 expression seen in FABP-deficient animals is highly relevant to their liver phenotype, since genetic SCD-1 deficiency also results in strong protection from hepatosteatosis and an overall phenotype reminiscent of FABP-deficient model presented here (Cohen et al., 2002). Finally, we demonstrate that aP2-mal1 deficiency results in decreased SREBP1c expression in liver and a consequent reduction in the transcriptional target genes for this key transcription factor for liver lipid metabolism. This is a likely response triggered by the elevated fatty acid levels delivered through the portal system to liver. Interestingly, however, SREBP2 expression is not altered by FABP deficiency. It has been shown that SREBP2 expression is upregulated in the liver tissue of SREBP1c-deficient mice, leading to increased liver cholesterol synthesis (Shimano et al., 1997). In the current model, despite decreased SREBP1c expression, there is no compensatory upregulation of SREBP2 in the liver tissue of aP2-mal1-deficient mice, which also provides further protection from hepatosteatosis with decreased HMG-CoA reductase and HMG-CoA synthase expression.

It is of note that both muscle AMP-K and liver SCD-1 have recently been established as major targets for peripheral leptin action. In this study, we also show data supporting enhanced activation of AMP-Kα1 and α2 isoforms in the muscle tissue of aP2-mal1$^{-/-}$ animals. Furthermore, AMP-K is also targeted by adiponectin, and adiponectin-stimulated AMP-Kα1 activity in muscle is also enhanced in aP2-mal1-deficient animals (data not shown). These observations raise the interesting possibility that at least part of the impact of FABPs on systemic metabolism is either dependent on leptin and/or adiponectin activity or mimicking peripheral actions of these molecules. Since there were no recognizable changes in food intake but a significant increase in energy expenditure in aP2-mal1$^{-/-}$ mice, we suggest that the primary site of action in these animals is at the periphery, whether or not it is dependent on leptin activity. Ad-

Table 1. Phenotypic comparison of single and combined FABP deficiency in mice

	aP2$^{-/-}$	mal1$^{-/-}$	aP2-mal1$^{-/-}$
Body weight	↑↑	↓	↓↓↓
Total adiposity	→	→	↓↓↓
Hepatosteatosis	→	→	↓↓↓↓
VCO_2	→	→	↑↑
VO_2	→	→	↑↑
ITT	↓↓	↓	↓↓↓↓
GTT	↓↓	↓	↓↓↓
Leptin	→	→	↓↓↓
Adiponectin	→	→	↓↓

The comparison represents the differences between genotypes in the context of dietary obesity. VCO_2, carbon dioxide production; VO_2, oxygen consumption; ITT, insulin tolerance test; GTT, glucose tolerance test. →, no change; ↑, increased; ↓, decreased; number of arrows indicates magnitude of change.

ditional studies in leptin- or adiponectin-deficient models could address these questions further.

We demonstrate significant alterations in fatty acid transport, availability, and composition upon loss of intracellular FABPs. These activities have not been associated with cytosolic FABPs in previous studies. Interestingly, since systemic free fatty acid levels are not decreased in FABP deficiency, our data supports the concept that transport and availability of fatty acids to the target tissues and the intracellular responses elicited by these lipids are more critical in determining the metabolic outcomes than the absolute values present in circulation. Regarding the latter, an interesting possibility remains that FABPs might also alter stress and inflammatory responses, including the activation of c-*jun* N-terminal kinase (Jnk) induced by lipids and cytokines, as well as ER stress, which are critically coupled to both obesity and insulin resistance (Hirosumi et al., 2002; Ozcan et al., 2004; Yuan et al., 2001). These observations should stimulate further interest in the important role played by these proteins in cellular and systemic lipid homeostasis.

In this study, we demonstrate that mice lacking the FABPs aP2 and mal1 are remarkably resistant to diet-induced obesity, fatty liver disease, insulin resistance, and type 2 diabetes. These results also illustrate that the aP2-mal1$^{-/-}$ mice differ from the individual deficiency of aP2 and mal1 in several respects (Table 1). First, whereas aP2-mal1$^{-/-}$ mice are protected from obesity, aP2- or mal1-deficient mice show no difference in systemic adiposity (Maeda et al., 2003), and aP2$^{-/-}$ mice actually gain more weight upon induction of dietary or genetic obesity (Hotamisligil et al., 1996; Scheja et al., 1999; Uysal et al., 2000). In addition, no difference in metabolic rates is observed in aP2- or mal1-deficient animals, whereas aP2-mal1-deficient animals exhibit increased O_2 consumption and CO_2 production. Second, the magnitude of the increase in insulin sensitivity observed in aP2-mal1 deficiency significantly exceeds that of individual aP2 or mal1 deficiency. There are also significant alterations in adipocytokine levels in aP2-mal$^{-/-}$ mice. Third, neither aP2 nor mal1 deficiency provides significant protection from hepatosteatosis, whereas this phenotype is essentially completely corrected in aP2-mal$^{-/-}$ animals. Hence, the molecular compensation observed in individual FABP deficiency models has substantial physiological significance.

Finally, in our earlier studies, we have also observed that FABP-deficient mice are dramatically protected against atherosclerosis through the action of these FABPs in macrophages (Boord et al., 2002, 2004; Makowski et al., 2001). These results clearly demonstrate that FABPs integrate metabolic and inflammatory responses in adipocytes and macrophages and that they are central to the development of key pathologies associated with metabolic syndrome. Taken together with the impact of FABPs on atherosclerosis, results presented here illustrate that blocking the activity of FABPs would constitute novel and powerful therapeutic opportunities, which could be exploited through straightforward biochemical assays based on ligand replacement, in obesity and associated disorders such as insulin resistance, type 2 diabetes, hepatosteatosis, and cardiovascular disease.

Experimental procedures

Mice and dietary studies

Mice with homozygous null mutations in aP2 and mal1 (aP2-mal1$^{-/-}$) were generated from an intercross between aP2$^{-/-}$ and mal1$^{-/-}$ mice, which resulted in double heterozygous mice and a subsequent crossing of aP2-mal1$^{-/+}$ animals with each other. All mice used in the study are males and backcrossed >12 generations into the C57BL/6J genetic background. The Institutional Animal Care and Use Committee (Harvard School of Public Health) approved all studies. To investigate the role of FABP deficiency in diet-induced obesity, we placed male, C57BL/6J-aP2$^{-/-}$, C57BL/6J-mal1$^{-/-}$, C57BL/6J-aP2-mal1$^{-/-}$, and C57BL/6J-wt control mice on a high-fat diet (Diet F3282, Bioserve, NJ) in which 50% of the calories are provided in the form of fat. This model of dietary obesity and insulin resistance is milder than that of the genetic models and considered similar to the extent of disease in the majority of humans (Uysal et al., 1997). Mice were placed on this diet at 4 weeks of age and followed until week 20. A control group on regular rodent diet was also included to determine the efficiency of the diet and comparisons with the obese group.

Imaging studies

T_2-weighted MR images were collected on a 4.7 T/40 cm horizontal bore Varian MR imager. Mice were positioned in a 3.8 cm imaging volume coil. The temperature inside the probe is maintained at 32°C. T_2-weighted imaging experiments were performed using a spin echo multislice sequence TR/TE = 2000/30 msec, 5 cm field of view, 128 × 128 matrix, and 2 mm slice thickness for axial images. Slices were collected to cover the regions of interest.

Metabolic studies

The details of indirect calorimetry and physical activity experiments are provided in the Supplemental Data. Tolerance tests were performed on male mice after 6 hr daytime food withdrawal. Insulin and glucose solutions were injected into peritoneal cavity at the dose of 0.5 U/kg and 1.0 mL/kg (1 M solution), respectively. Blood was collected via tail vein at different time points, and glucose levels were measured by the use of a glucometer (Precision). Serum insulin, leptin, and adiponectin levels were measured

with RIAs for rat insulin and mouse leptin and adiponectin (Linco Research). Serum lipid concentrations were determined by established assays as previously described (Maeda et al., 2003; Uysal et al., 2000).

Liver and muscle triglycerides, fatty acid analysis, and treatments

Soleus muscle was carefully dissected from mice to limit fat contamination. Triglyceride in soleus muscle or liver tissue was determined using a commercial kit (Determiner TG, Kyoma Medex, Japan). Total lipids were extracted from serum by the method of Dole and Meinertz (1960). Free fatty acids were separated from esterified fatty acids by thin layer chromatography using silica gel and a mixture of petroleum ether:diethyl ether: acetic acid (80:20:1) as the stationary and mobile phases, respectively. Fatty acids were methylated by incubation (50°C, 1 hr) with methanol/acetyl chloride (20:1), evaporated, redissolved in isooctane, and separated by gas chromatography. Individual fatty acids were identified by comparison to purified standards. C2C12 myoblasts were cultured in DMEM containing 10% fetal bovine serum, and differentiation was induced by DMEM supplemented with 2% horse serum. Cells were treated with fatty acids, as described (Chavez and Summers, 2003). On day 4 of differentiation, cells were incubated with indicated fatty acid (0.75 mM in DMEM with 1% FBS, 2% BSA) for 20 hr. Cells were changed into serum-free medium containing the same fatty acid 4 hr prior to experiment and then treated with or without insulin (100 nM, 10 min). L6 cells were cultured and differentiated as described (Tong et al., 2001) and treated with fatty acids on day 7. Fao cells maintained in DMEM with 10% FBS were washed with PBS twice and treated with free fatty acids in DMEM with 2% BSA for 24 hr.

Fatty acid binding and uptake assay

FA binding activity was determined as described (Glatz and Veerkamp, 1983) using Lipidex. The detailed protocol is provided in the Supplemental Data. For uptake experiments, epididymal fat pads from five to six 12-week-old mice were collected and digested with collagenase. The floating adipocytes were washed three times with Krebs-Ringer phosphate isolation buffer containing 20 mM HEPES (pH 7.4), 2.5% BSA, 200 μM adenosine, and 5 mM glucose. Cell suspension (200 μl) was incubated with ^{3}H-labeled lauric, myristic, palmitic, or stearic acid at a final concentration of 100 μM at 37°C for 30 min. Following the incubation, the uptake was terminated by adding ice-cold stop solution containing 0.1% BSA and 200 μM phloretin in isolation buffer. The cell suspension was then transferred onto a Whatman glass filter and washed three times with ice-cold PBS. The radioactivity of the filters was measured by a liquid scintillation counter.

Glucose uptake, AMP-K enzyme activity, and fatty acid oxidation

Glucose uptake assays in muscle strips and primary adipocytes were performed as described (Abel et al., 2001; Bruning et al., 1998). For AMP-K enzyme assay, mice were housed in individual cages and, 5 days before the experiment, indwelling catheters were implanted into the jugular vein. Injection of leptin or saline was initiated from 9 to 10 a.m. (lights on, 6 a.m.). Food and water were available during the experiments. Recombinant murine leptin (1 mg/kg body weight) (Peprotech) was injected intravenously through the jugular vein catheter in mice anesthetized with ketamine (40 mg/kg) and xylazine (5 mg/kg) solution. Control mice received the same volume of saline. After the mice were sacrificed, skeletal muscles were rapidly dissected and frozen in liquid nitrogen. To measure isoform-specific AMP-K activity, AMP-K was immunoprecipitated from muscle lysates (100 μg of protein) with specific antibodies against the α1 or α2 catalytic subunits (gift of Dr. Carling) bound to protein G-Sepharose beads. Kinase activity was measured using synthetic "SAMS" peptide and [γ-^{32}P]-ATP, as described (Minokoshi et al., 2002). Fatty acid oxidation activity in muscle was determined by a previously described method (Kaushik et al., 2001) with modifications, which is detailed in the Supplemental Data.

SCD activity, immunoblotting, and gene expression analysis

SCD activity was determined from the production of $^{3}H_2O$ using [9, 10-^{3}H]-stearoyl-CoA as substrate (Gomez et al., 2002). Tissues were homogenized, and the microsomal fractions (105,000 × g) were isolated by sequential centrifugations. Reactions were performed at 37°C for 30 min with 100 μg/mL protein homogenate, 10 μM (2 uCi/mL) of [9, 10-^{3}H]-stearoyl-CoA (American Radiolabeled Chemicals Inc.), and 30 μM NADH in 100 μl of 10 mM potassium phosphate buffer (pH 7.4). After the reaction, 100 μl of 10 mg/mL fatty acid-free BSA (Sigma) and 200 μl of 10% trichloroacetic acid were added and then mixed. After centrifugation (5000 × g, 10 min), radioactive counts in the supernatant were measured by a scintillation counter. The enzyme activity was expressed as nmol min^{-1} mg^{-1} protein. FABP proteins were detected by immunoblotting with antisera raised against full-length human mal1 and aP2 in adipose tissue extracts prepared as described (Scheja et al., 1999). Phosphorylation of the α subunit of AMP-K in soleus lysates was determined with gradient SDS-PAGE gels using an antibody against phosphopeptides based on the amino acid sequence surrounding Thr172 of either α1 and α2 isoforms of the catalytic subunit of AMP-K (Cell Signaling). Protein levels of AMP-K were determined using an antibody for both α1 and α2 subunits of AMP-K (Cell Signaling). AKT and phospho-AKT antibodies were purchased from Cell Signaling. RNA extraction and gene expression studies are detailed in the Supplemental Data.

Statistical analysis

All numerical data were expressed as mean, and error bars represent the SEM. Two-tailed, two-sample, unequal variance Student's t tests were used to assess statistical significance where $p < 0.05$ was the accepted level of statistical significance.

Supplemental data

Supplemental Data include one figure, two tables, Supplemental Experimental Procedures, and Supplemental References and can be found with this article online at http://www.cellmetabolism.org/cgi/content/full/1/2/107/DC1/.

Acknowledgments

This work was supported in part by grants from NIH (DK64360 to G.S.H. and DK56116 and DK57521 to B.B.K.) and Pew Foundation and American Diabetes Association (G.S.H.). K.M. is recipient of a fellowship from Manpei Suzuki Diabetes Foundation, H.C. is recipient of a mentor-based fellowship from American Diabetes Association, M.F. is recipient of a fellowship from the Japan Society for the Promotion of Science, and Q.C. is supported by NIH training grant T32-DK07703. We thank Laurie Goodyear's lab for help in setting up the uptake and oxidation assays in muscle and Franks Sacks and Hannia Campos for help in fatty acid composition analysis. H.M., B.K., and R.A.P. are employed by a for profit company developing drugs for diabetes.

Received: July 23, 2004
Revised: November 23, 2004
Accepted: December 22, 2004
Published: February 15, 2005

References

Abel, E.D., Peroni, O., Kim, J.K., Kim, Y.B., Boss, O., Hadro, E., Minnemann, T., Shulman, G.I., and Kahn, B.B. (2001). Adipose-selective targeting of the GLUT4 gene impairs insulin action in muscle and liver. Nature *409*, 729–733.

Arita, Y., Kihara, S., Ouchi, N., Takahashi, M., Maeda, K., Miyagawa, J., Hotta, K., Shimomura, I., Nakamura, T., Miyaoka, K., et al. (1999). Paradoxical decrease of an adipose-specific protein, adiponectin, in obesity. Biochem. Biophys. Res. Commun. *257*, 79–83.

Bernlohr, D.A., Coe, N.R., and LiCata, V.J. (1999). Fatty acid trafficking in the adipocyte. Semin. Cell Dev. Biol. *10*, 43–49.

Boord, J.B., Maeda, K., Makowski, L., Babaev, V.R., Fazio, S., Linton, M.F., and Hotamisligil, G.S. (2002). Adipocyte fatty acid-binding protein, aP2, alters late atherosclerotic lesion formation in severe hypercholesterolemia. Arterioscler. Thromb. Vasc. Biol. *22*, 1686–1691.

Boord, J.B., Maeda, K., Makowski, L., Babaev, V.R., Fazio, S., Linton, M.F., and Hotamisligil, G.S. (2004). Combined adipocyte-macrophage fatty acid-binding protein deficiency improves metabolism, atherosclerosis, and survival in apolipoprotein E-deficient mice. Circulation *110*, 1492–1498.

Bruning, J.C., Michael, M.D., Winnay, J.N., Hayashi, T., Horsch, D., Accili, D., Goodyear, L.J., and Kahn, C.R. (1998). A muscle-specific insulin receptor knockout exhibits features of the metabolic syndrome of NIDDM without altering glucose tolerance. Mol. Cell *2*, 559–569.

Chavez, J.A., and Summers, S.A. (2003). Characterizing the effects of saturated fatty acids on insulin signaling and ceramide and diacylglycerol accumulation in 3T3-L1 adipocytes and C2C12 myotubes. Arch. Biochem. Biophys. *419*, 101–109.

Cohen, P., Miyazaki, M., Socci, N.D., Hagge-Greenberg, A., Liedtke, W., Soukas, A.A., Sharma, R., Hudgins, L.C., Ntambi, J.M., and Friedman, J.M. (2002). Role for stearoyl-CoA desaturase-1 in leptin-mediated weight loss. Science *297*, 240–243.

Dole, V.P., and Meinertz, H. (1960). Microdetermination of long-chain fatty acids in plasma and tissues. J. Biol. Chem. *235*, 2595–2599.

Flegal, K.M., Carroll, M.D., Kuczmarski, R.J., and Johnson, C.L. (1998). Overweight and obesity in the United States: prevalence and trends, 1960–1994. Int. J. Obes. Relat. Metab. Disord. *22*, 39–47.

Friedman, J.M., and Halaas, J.L. (1998). Leptin and the regulation of body weight in mammals. Nature *395*, 763–770.

Fruebis, J., Tsao, T.S., Javorschi, S., Ebbets-Reed, D., Erickson, M.R., Yen, F.T., Bihain, B.E., and Lodish, H.F. (2001). Proteolytic cleavage product of 30-kDa adipocyte complement-related protein increases fatty acid oxidation in muscle and causes weight loss in mice. Proc. Natl. Acad. Sci. USA *98*, 2005–2010.

Glatz, J.F., and Veerkamp, J.H. (1983). A radiochemical procedure for the assay of fatty acid binding by proteins. Anal. Biochem. *132*, 89–95.

Gomez, F.E., Miyazaki, M., Kim, Y.C., Marwah, P., Lardy, H.A., Ntambi, J.M., and Fox, B.G. (2002). Molecular differences caused by differentiation of 3T3-L1 preadipocytes in the presence of either dehydroepiandrosterone (DHEA) or 7-oxo-DHEA. Biochemistry *41*, 5473–5482.

Hirosumi, J., Tuncman, G., Chang, L., Gorgun, C.Z., Uysal, K.T., Maeda, K., Karin, M., and Hotamisligil, G.S. (2002). A central role for JNK in obesity and insulin resistance. Nature *420*, 333–336.

Hotamisligil, G.S., Johnson, R.S., Distel, R.J., Ellis, R., Papaioannou, V.E., and Spiegelman, B.M. (1996). Uncoupling of obesity from insulin resistance through a targeted mutation in aP2, the adipocyte fatty acid binding protein. Science *274*, 1377–1379.

Kaushik, V.K., Young, M.E., Dean, D.J., Kurowski, T.G., Saha, A.K., and Ruderman, N.B. (2001). Regulation of fatty acid oxidation and glucose metabolism in rat soleus muscle: effects of AICAR. Am. J. Physiol. Endocrinol. Metab. *281*, E335–E340.

Maeda, K., Uysal, K.T., Makowski, L., Gorgun, C.Z., Atsumi, G., Parker, R.A., Bruning, J., Hertzel, A.V., Bernlohr, D.A., and Hotamisligil, G.S. (2003). Role of the fatty acid binding protein mal1 in obesity and insulin resistance. Diabetes *52*, 300–307.

Makowski, L., Boord, J.B., Maeda, K., Babaev, V.R., Uysal, K.T., Morgan, M.A., Parker, R.A., Suttles, J., Fazio, S., Hotamisligil, G.S., and Linton, M.F. (2001). Lack of macrophage fatty-acid-binding protein aP2 protects mice deficient in apolipoprotein E against atherosclerosis. Nat. Med. *7*, 699–705.

Matsuzawa, Y., Funahashi, T., and Nakamura, T. (1999). Molecular mechanism of metabolic syndrome X: contribution of adipocytokines adipocyte-derived bioactive substances. Ann. N Y Acad. Sci. *892*, 146–154.

Minokoshi, Y., Kim, Y.B., Peroni, O.D., Fryer, L.G., Muller, C., Carling, D., and Kahn, B.B. (2002). Leptin stimulates fatty-acid oxidation by activating AMP-activated protein kinase. Nature *415*, 339–343.

Muoio, D.M., Dohm, G.L., Fiedorek, F.T., Jr., Tapscott, E.B., Coleman, R.A., and Dohn, G.L. (1997). Leptin directly alters lipid partitioning in skeletal muscle. Diabetes *46*, 1360–1363.

Ozcan, U., Cao, Q., Yilmaz, E., Lee, A.H., Iwakoshi, N.N., Ozdelen, E., Tuncman, G., Gorgun, C., Glimcher, L.H., and Hotamisligil, G.S. (2004). Endoplasmic reticulum stress links obesity, insulin action, and type 2 diabetes. Science *306*, 457–461.

Razani, B., Combs, T.P., Wang, X.B., Frank, P.G., Park, D.S., Russell, R.G., Li, M., Tang, B., Jelicks, L.A., Scherer, P.E., and Lisanti, M.P. (2002). Caveolin-1-deficient mice are lean, resistant to diet-induced obesity, and show hypertriglyceridemia with adipocyte abnormalities. J. Biol. Chem. *277*, 8635–8647.

Saltiel, A.R. (2001). New perspectives into the molecular pathogenesis and treatment of type 2 diabetes. Cell *104*, 517–529.

Scheja, L., Makowski, L., Uysal, K.T., Wiesbrock, S.M., Shimshek, D.R., Meyers, D.S., Morgan, M., Parker, R.A., and Hotamisligil, G.S. (1999). Altered insulin secretion associated with reduced lipolytic efficiency in aP2–/– mice. Diabetes *48*, 1987–1994.

Sethi, J.K., and Hotamisligil, G.S. (1999). The role of TNF alpha in adipocyte metabolism. Semin. Cell Dev. Biol. *10*, 19–29.

Shimano, H., Shimomura, I., Hammer, R.E., Herz, J., Goldstein, J.L., Brown, M.S., and Horton, J.D. (1997). Elevated levels of SREBP-2 and cholesterol synthesis in livers of mice homozygous for a targeted disruption of the SREBP-1 gene. J. Clin. Invest. *100*, 2115–2124.

Shulman, G.I. (2000). Cellular mechanisms of insulin resistance. J. Clin. Invest. *106*, 171–176.

Sjogren, K., Hellberg, N., Bohlooly, Y.M., Savendahl, L., Johansson, M.S., Berglindh, T., Bosaeus, I., and Ohlsson, C. (2001). Body fat content can be predicted in vivo in mice using a modified dual-energy X-ray absorptiometry technique. J. Nutr. *131*, 2963–2966.

Skyler, J.S., and Oddo, C. (2002). Diabetes trends in the USA. Diabetes Metab. Res. Rev. *131*, S21–S26.

Soukas, A., Cohen, P., Socci, N.D., and Friedman, J.M. (2000). Leptin-specific patterns of gene expression in white adipose tissue. Genes Dev. *14*, 963–980.

Spiegelman, B.M., and Flier, J.S. (2001). Obesity and the regulation of energy balance. Cell *104*, 531–543.

Tilg, H., and Diehl, A.M. (2000). Cytokines in alcoholic and nonalcoholic steatohepatitis. N. Engl. J. Med. *343*, 1467–1476.

Tong, P., Khayat, Z.A., Huang, C., Patel, N., Ueyama, A., and Klip, A. (2001). Insulin-induced cortical actin remodeling promotes GLUT4 insertion at muscle cell membrane ruffles. J. Clin. Invest. *108*, 371–381.

Uysal, K.T., Wiesbrock, S.M., Marino, M.W., and Hotamisligil, G.S. (1997). Protection from obesity-induced insulin resistance in mice lacking TNF-alpha function. Nature *389*, 610–614.

Uysal, K.T., Scheja, L., Wiesbrock, S.M., Bonner-Weir, S., and Hotamisligil, G.S. (2000). Improved glucose and lipid metabolism in genetically obese mice lacking aP2. Endocrinology *141*, 3388–3396.

Winder, W.W., and Hardie, D.G. (1999). AMP-activated protein kinase, a metabolic master switch: possible roles in type 2 diabetes. Am. J. Physiol. *277*, E1–10.

Yamauchi, T., Kamon, J., Waki, H., Terauchi, Y., Kubota, N., Hara, K., Mori, Y., Ide, T., Murakami, K., Tsuboyama-Kasaoka, N., et al. (2001). The fat-derived hormone adiponectin reverses insulin resistance associated with both lipoatrophy and obesity. Nat. Med. *7*, 941–946.

Yuan, M., Konstantopoulos, N., Lee, J., Hansen, L., Li, Z.W., Karin, M., and Shoelson, S.E. (2001). Reversal of obesity- and diet-induced insulin resistance with salicylates or targeted disruption of Ikkbeta. Science *293*, 1673–1677.

Zimmet, P., Alberti, K.G., and Shaw, J. (2001). Global and societal implications of the diabetes epidemic. Nature *414*, 782–787.